Crystal structure of the stimulatory complex of GTP cyclohydrolase I and its feedback regulatory protein GFRP

Nobuo Maita*, Kengo Okada*, Kazuyuki Hatakeyama†‡, and Toshio Hakoshima*‡

*Department of Molecular Biology, Nara Institute of Science and Technology, 8916-5 Takayama, Ikoma, Nara 630-0101, Japan; and †Department of Surgery, University of Pittsburgh, Pittsburgh, PA 15213

Communicated by Yasuyuki Yamada, Nara Institute of Science and Technology, Nara, Japan, December 4, 2001 (received for review September 25, 2001)

In the presence of phenylalanine, GTP cyclohydrolase I feedback regulatory protein (GFRP) forms a stimulatory 360-kDa complex with GTP cyclohydrolase I (GTPCHI), which is the rate-limiting enzyme in the biosynthesis of tetrahydrobiopterin. The crystal structure of the stimulatory complex reveals that the GTPCHI decamer is sandwiched by two GFRP homopentamers. Each GFRP pentamer forms a symmetrical five-membered ring similar to β-propeller. Five phenylalanine molecules are buried inside each interface between GFRP and GTPCHI, thus enhancing the binding of these proteins. The complex structure suggests that phenylalanine-induced GTPCHI·GFRP complex formation enhances GTPCHI activity by locking the enzyme in the active state.

In animals, tetrahydrobiopterin (BH_4) is an essential cofactor for key enzymes producing nitric oxide and neurotransmitters such as catecholamines and serotonin and thus is involved in diverse body functions including neurotransmission, blood pressure regulation, immune function, and the conversion of phenylalanine to tyrosine. GTP cyclohydrolase I (GTPCHI, EC 3.5.4.16) catalyzes the initial step in the *de novo* synthesis of BH_4 from GTP (Fig. 1). Genetic defects affecting GTPCHI activity cause hyperphenylalaninemia and severe neurological disorders such as 3,4-dihydroxyphenylalanine-responsive dystonia (1–4). The BH_4 deficiency that occurs because of abnormalities in the control mechanisms of GTPCHI have been found in a variety of diseases ranging from vascular diseases such as diabetes, hypertension, and atherosclerosis (5–8) to neurological diseases such as Parkinson's and Alzheimer's (9, 10). Recent findings that guanine and 8-hydroxyguanine inhibit GTPCHI activity in a GTPCHI feedback regulatory protein (GFRP)-dependent manner raise the possibility that a BH_4 deficiency occurs in Lesch–Nyhan syndrome and Parkinson's disease (11). These facts underscore the physiological and pathophysiological importance of BH_4 production.

The identification of GFRP, which functions as both a positive and negative regulator of GTPCHI, has revealed the tight regulation of GTPCHI activity that maintains intracellular BH_4 levels at and below those needed by BH_4-requiring enzymes (12). GFRP mediates feed-forward activation of GTPCHI activity by enhancing GTP binding in the presence of phenylalanine while it induces feedback inhibition of enzyme activity in the presence of BH_4. Phenylalanine is the first substrate for BH_4-requiring hydroxylases in the metabolic pathway producing 3,4-dihydroxyphenylalanine (Fig. 1). The effects of GFRP on GTPCHI occur via phenylalanine- or BH_4-dependent protein complex formation between GTPCHI and GFRP (12, 13). In the absence of GFRP, phenylalanine has no effect on GTPCHI activity, which displays typical allosteric enzyme kinetics with strong positive cooperativity with GTP, the substrate (12, 14). Phenylalanine and GFRP reduce the positive cooperativity of GTPCHI and, as a result, stimulate the enzyme's activity in the presence of subsaturating concentrations of GTP.

GTPCHI is a decamer of 260 kDa with a subunit consisting of 230 amino acid residues (15), and GFRP is a pentamer of 50 kDa with a subunit consisting of 83 amino acid residues (16). Recently, we showed that both stimulatory and inhibitory GTPCHI·GFRP complexes consist of one molecule of decameric GTPCHI and two molecules of pentameric GFRP (13). Here we describe the crystal structure of the phenylalanine-induced stimulatory complex formed between rat GFRP and GTPCHI. The structure reveals a β-propeller-like structure of the GFRP pentamer as well as a higher order architecture involving the assembly of a 360-kDa complex formed by two GFRP pentamers bound to each of the outer faces of the GTPCHI decamer. The structure described here also reveals the binding of 10 molecules of phenylalanine to the complex at interfaces between GTPCHI and GFRP. On the basis of the complex structure compared with other GTPCHI structures, we consider the possible mechanism of allosteric regulation of this enzyme system.

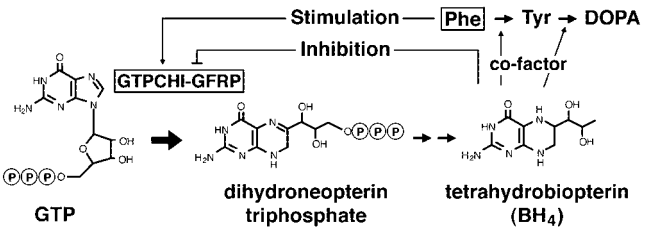

Fig. 1. Reaction scheme and regulation mechanisms of the GTPCHI·GFRP complex. DOPA, 3,4-dihydroxyphenylalanine.

Materials and Methods

Protein Purification, Crystallization, and Data Collection. Rat recombinant GTPCHI and GFRP were expressed in *Escherichia coli* cells, purified, and crystallized as described (13, 16, 17). The stimulatory complex (5 mg/ml) was crystallized from 24% (vol/vol) 2-methyl-2,4-pentanediol/75 mM Tris·HCl (pH 7.5)/50 mM KCl/5 mM phenylalanine. The space group is $P2_1$ with unit cell dimensions a = 123.2 Å, b = 111.4 Å, c = 125.8 Å, and β = 97.69°. The selenomethionine-substituted GFRP was prepared, and the stimulatory complex crystals including selenomethionine GFRP were used as heavy-atom derivative. The CH_3HgCl derivative was prepared by soaking the native crystals of stimulatory complex in 5 μl of droplets containing 1 mM CH_3HgCl, 40% (vol/vol) 2-methyl-2,4-pentanediol, 5 mM phenylalanine,

Abbreviations: BH_4, tetrahydrobiopterin; GTPCHI, GTP cyclohydrolase I; GFRP, GTPCHI feedback regulatory protein.

Data deposition: The atomic coordinates and structure factors have been deposited in the Protein Data Bank, www.rcsb.org (PDB ID codes 1IS7 and 1IS8).

‡To whom reprint requests may be addressed. E-mail: hakosima@bs.aist-nara.ac.jp or hatakeya+@imap.pitt.edu.

The publication costs of this article were defrayed in part by page charge payment. This article must therefore be hereby marked "*advertisement*" in accordance with 18 U.S.C. §1734 solely to indicate this fact.

Table 1. Crystallographic and refinement statistics

		Native 1	Seleno-methionyl	CH_3HgCl	Native 2
Data collection*	X-ray source/wavelength, Å	PF/0.980	SPring-8/1.000	In House/1.542	SPring-8/1.282
	Resolution, Å	3.0 (3.11–3.00)	2.8 (2.94–2.80)	3.5 (3.62–3.50)	2.7 (2.84–2.70)
	Reflections, observed/unique	368,952/60,761	589,690/83,068	36,708/2,949	693,751/93,244
	R_{sym}, %†	6.8 (25.9)	11.2 (57.8)	13.2 (26.7)	9.5 (28.6)
	Completeness, %	89.4 (72.8)	99.4 (99.4)	85.8 (69.6)	99.9 (99.9)
Phasing	Resolution range, Å		15.0–3.1	15.0–3.5	
	Heavy atom sites		27 (of 50)	10	
	R_{deriv}, %‡		16.9	4.2	
	R_{Cullis}, centric/acentric§		0.92/0.94	0.90/0.81	
	Phasing power, centric/acentric¶		0.45/0.64	0.88/1.19	
	Overall figure of merit		0.79		
Model refinement	Resolution range, Å		15–2.8		15–2.7
	R_{work}/R_{free}, %‖		22.8/26.4		21.6/24.3
	B_{ave}, Å^2		57.2		42.6
	Rms deviation bond lengths, Å/bond angles, °		0.0083/1.35		0.0082/1.39
	No. of atoms, protein/solvent		22,120/272		22,000/512

*Statistics for the outer shell are given in parentheses.

†$R_{sym} = \Sigma_{hkl}\Sigma_i|I_{mean} - I_i|/\Sigma_{hkl}\Sigma_i I_i$.

‡$R_{deriv} = \Sigma||F_{derivative}| - |F_{native}||/\Sigma|F_{native}|$.

§$R_{Cullis} = \Sigma||F_{PH}| \pm |F_P| - |F_{H(calc)}||/\Sigma||F_{PH}| \pm |F_P||$, where F_{PH}, F_P, and F_H are the scaled structure factors of the derivative, native, and heavy atom, respectively.

¶Phasing power = $\langle F_H \rangle / \langle$lack of closure$\rangle$.

‖$R_{work/free} = \Sigma||F_O| - |F_C||/\Sigma|F_O|$, where F_O and F_C are the observed and calculated structure factor amplitudes, respectively. 5% of the reflections were excluded from the working set for calculating the free R value.

and 0.1 M Tris·HCl (pH 7.5) at 4°C for 13 h. The intensity data of the native (Native 1) and selenomethionyl derivative crystals were collected at 100 K at the Photon Factory (BL 6a and 18b, Tsukuba, Japan) and SPring-8 (BL41XU, Harima, Japan), respectively. The data set of the methylmercurychloride derivative was collected with an R-AXIS IV imaging plate detector on a Rigaku (Tokyo) FR-C (λ = 1.542 Å). The data-collection statistics are summarized in Table 1.

Structure Determination and Model Building. Initially, the molecular replacement trials were attempted by using the *E. coli* GTPCHI structure (PDB code 1GTP; ref. 18) with AMORE (19). However, the molecular replacement solution gave a Fourier map that was not of high enough quality to trace the polypeptide chain of GFRP. The complex structure was solved by the multiple isomorphous replacement method by using the native data set (Native 1) with the methylmercurychloride and selenomethionyl derivatives. There were 10 mercury sites in the asymmetric unit; two sets of five sites are related to the noncrystallographic 5-fold rotation symmetry. These sites were confirmed in a difference Fourier map calculated with the molecular replacement phases. By using the phases calculated from the mercury sites, 27 of 50 selenium sites were found in a difference Fourier map. The initial phases were calculated and refined with MLPHARE (20). The density modification, including noncrystallographic symmetry averaging, histogram matching and solvent flattening, and phase extension greatly improved the phases and produced an excellent electron density map, in which most of the GFRP residues could be built unambiguously with O (21). The phasing statistics are summarized in Table 1.

Structure Refinement. First, the structure refinement was carried out with CNS (22) by using the selenomethionyl derivative data at 2.8-Å resolution. Rounds of manual rebuilding and structure refinement by using a maximum-likelihood target gave a final refined model of the stimulatory complex with an R factor of 22.8% (R_{free} factor of 26.4%) including 2,780 amino acids of the GTPCHI·GFRP complex, 10 phenylalanines, 142 water molecules, and 10 tentative potassium ions but a 2Fo-Fc map containing poor peaks for zinc ions at the active sites. After the refinement, a 2.7-Å native data set (Native 2) was collected from the complex crystals that were prepared with a GTPCHI sample purified without EDTA. The identification of zinc ions was performed by x-ray absorption fine-structure measurements and by a difference Fourier map calculated with the data set collected with a wavelength (λ = 1.2818 Å) for the absorption edge of zinc atoms. Structural refinements against this native data to an R factor of 21.6% (R_{free} 24.3%) revealed 10 zinc ions at the active sites. All residues of each GFRP were ordered in the electron density map, whereas the 47 N-terminal residues of each GTPCHI and two GTPCHI residues (Val-209 and Gln-210) were not visible, probably because of disorder. In the refined structure of the selenomethionyl derivative, Gln-80 was replaced with Ala.

Figs. 2 *A* and *B* were drawn by RASMOL (www.bernstein-plus-sons.com/software/rasmol), and Figs. 2*C*, 3*B*, 4, 5*D*, 6, and 7 were created with MOLSCRIPT (23) and RASTER3D (24). Figs. 5 *A*, *B*, and *C* were made with GRASP (25).

Results and Discussion

Overall Structure. The crystal contains one complex formed by the GTPCHI decamer, two GFRP pentamers, and ten phenylalanine molecules in an asymmetric unit. The model includes 10 GTPCHI subunits (residues 48–241), 10 GFRP subunits (residues 1–84), 10 phenylalanine molecules, and 10 zinc ions. The 47 residues of each GTPCHI at the N terminus were not defined in the current electron density map, probably because of disorder. However, it has been suggested that this region has little effect on the activity of this enzyme (26). It has been suggested also that the N-terminal region plays only a small role in feedback regulation by GFRP (16, 26).

The stimulatory GTPCHI·GFRP complex consists of three layers, $(GFRP)_5$-$(GTPCHI)_{10}$-$(GFRP)_5$, with overall dimensions of ≈130-Å height and 93-Å diameter (Fig. 2 *A* and *B*). GFRP forms a pentamer that is arranged as a compact ring (with a 56-Å diameter and a 32-Å height), as suggested by a previous study using gel filtration (16). The GTPCHI decamer consists of two homopentameric rings and forms a torus-shaped structure with dimensions of 93 Å in diameter and 66 Å in height. Two GFRP pentamers interact with top and bottom molecular sur-

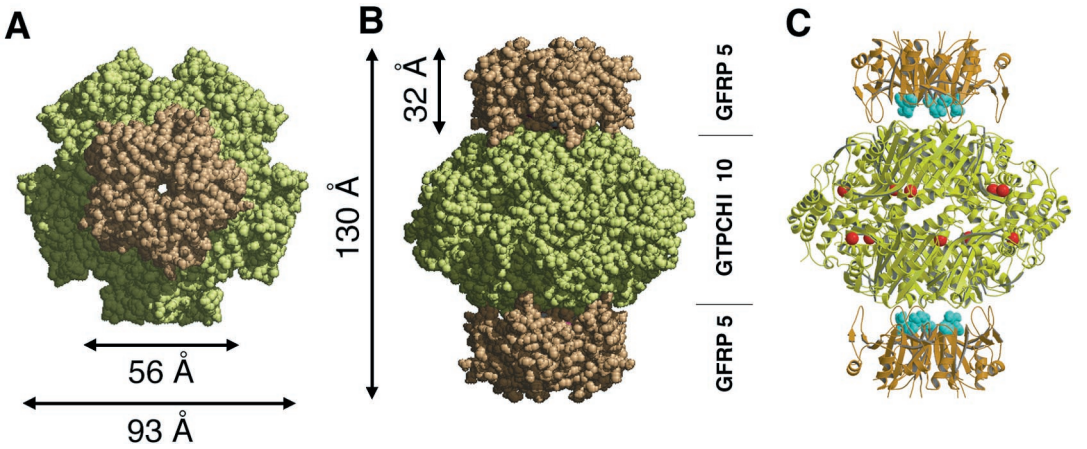

Fig. 2. Overall structure of the stimulatory GTPCHI·GFRP complex. Top (*A*) and side (*B*) views of a space-filled model of the stimulatory GTPCHI·GFRP complex, respectively, are shown. The two GFRP pentamers are shown in light orange, and the GTPCHI decamer is shown in amber. The complex model in *A* is viewed from the 5-fold axis, and *B* is viewed from one of the 2-fold axes. (*C*) A side view of a ribbon representation of the stimulatory GTPCHI·GFRP complex. The phenylalanine molecules are shown as space-filled models (blue), which are located at the interfaces between GFRP and GTPCHI. Zinc ions located at the active sites are shown as red balls.

faces of the torus-shaped GTPCHI decamer, sharing the same 5-fold axis. At each interface between GFRP and GTPCHI, five phenylalanine molecules are located (Fig. 2*C*). This binding stoichiometry of phenylalanine is consistent with that determined by the equilibration gel filtration method by Hummel and Dreyer (27). Each active site of the GTPCHI monomer contains one zinc ion.

GFRP Structure. The GFRP monomer consists of a six-stranded antiparallel β-sheet and two α-helices. These secondary structure elements are arranged into a $\beta\beta\alpha\beta\beta\alpha\beta\beta$ topology, which could belong to the ($\alpha + \beta$) protein class in the SCOP classification (ref. 28; Fig. 3 *A*–*C*). A DALI (29) search reveals the highest structural similarity with a *Z* score of 3.8 for a yeast protein YciH (30), which is a product from a structural genomics

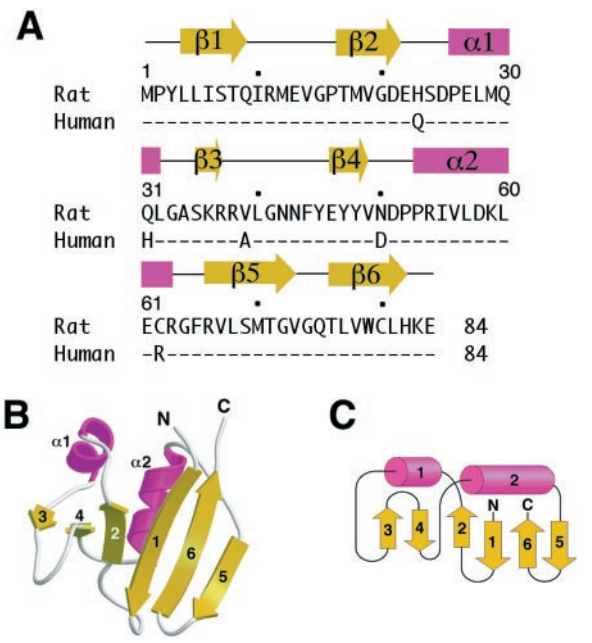

Fig. 3. The GFRP structure. (*A*) The secondary structure elements of the rat GFRP monomer and amino acid sequence alignment of rat and human GFRP. Identical residues are marked with a dash (−). GFRP contains two α-helices (pink rectangles) and six β-strands (yellow arrows). Human GFRP has the same chain length (84 residues) as rat GFRP and shares 94% sequence homology. (*B*) A ribbon representation of the GFRP monomer. (*C*) The topology map of the GFRP monomer. Helices and strands are shown in the same colors as those used for *A*.

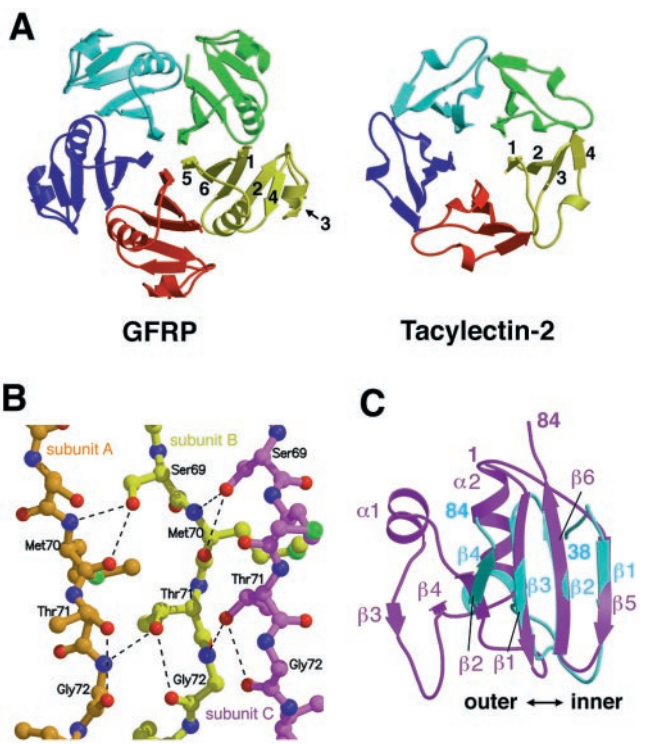

Fig. 4. (*A*) A comparison of GFRP and tachylectin-2 with top views of GFRP (*Left*) and tachylectin-2 (*Right*; PDB code 1TL2). The five GFRP monomers and each blade of tachylectin-2 are shown in different colors. The strand numbers are indicated also. (*B*) A close-up view of the β5 strands of GFRP located at the center of the pentameric ring. For clarity, three strands from different GFRP monomers are drawn as ball-and-stick models using different colors. Hydrogen bonds involving the side chains of Ser-69 and Thr-71 are indicated by broken lines. (*C*) Superimposition of the GFRP subunit (magenta) onto a blade of tachylectin-2 (blue).

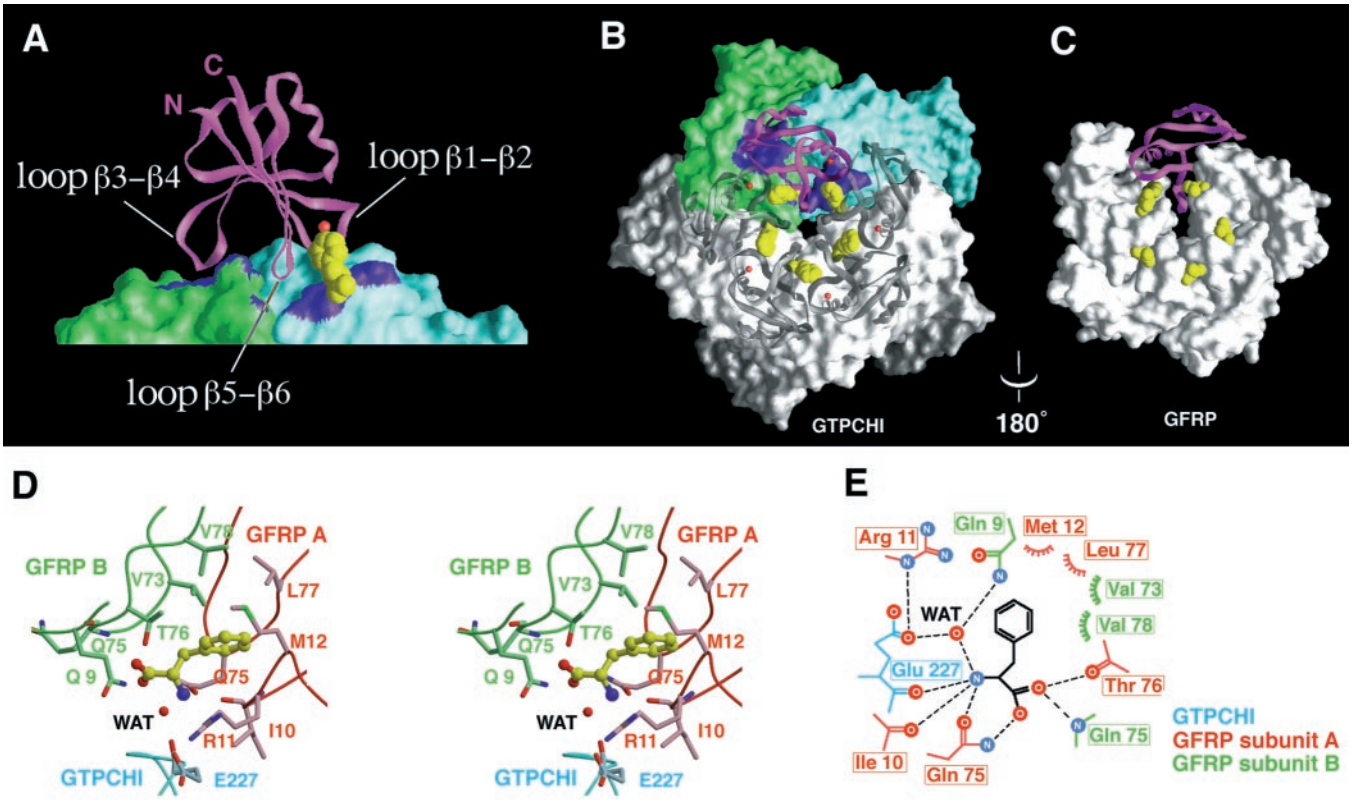

Fig. 5. The phenylalanine-binding sites at the interfaces between GFRP and GTPCHI. (*A* and *B*) The contacts between GFRP and GTPCHI are shown with ribbon models of the GFRP subunits and molecular surfaces of GTPCHI. (*A*) A close-up side view of one GFRP subunit (magenta) that makes contact with two GTPCHI subunits (green and light blue). (*B*) A top view of the GFRP pentamer on the GTPCHI decamer. In both panels, molecular surfaces colored in blue indicate the GTPCHI residues contacting GFRP. The bound phenylalanine molecules are shown as space-filled models (yellow). The tentative potassium ions are shown as red balls. (*C*) Five phenylalanine molecules bound to the stimulatory complex are depicted on the molecular surfaces of the GFRP pentamer with one GFRP monomer as a ribbon model (magenta). The bound phenylalanine molecules are shown as space-filled models (yellow). (*D*) A close-up stereoview of the phenylalanine-binding site located at the interfaces formed by two GFRP subunits (red and pale green) and one GTPCHI subunit (blue). The bound phenylalanine molecule is shown as a ball-and-stick model (yellow). The bridging water molecule is shown as a red ball with the label WAT. (*E*) Schematic representation of the GFRP– and GTPCHI–phenylalanine interactions. Broken lines indicate hydrogen bonds. The two GFRP subunits are colored in red and pale green, and one GTPCHI subunit is colored in blue. The bound phenylalanine molecule is shown in black lines. The bridging water molecule is labeled WAT.

project, the function of which remains unknown. YciH lacks a β-strand corresponding to the C-terminal strand of GFRP.

Surprisingly, the architecture of the GFRP pentameric ring (Fig. 4*A*, *Left*) is very similar to the β-propeller domains found in several proteins such as tachylectin-2 (ref. 31; Fig. 4*A*, *Right*) and G_β subunit (32), containing characteristic sequence repeats of $\approx$50 residues in a single polypeptide chain (33). To date, β-propeller structures with a 4–8-fold propeller geometry have been found in functionally unrelated proteins including a lectin tachylectin-2, which displays a 5-fold β-propeller. Each GFRP monomer corresponds to a blade of the propeller, which is formed by each repeat in the classical β-propeller protein. Thus, in contrast to these proteins that have blades in a single polypeptide chain, GFRP provides an example of a homooligomeric β-propeller structure.

The GFRP pentamer exhibits several remarkable features distinct from those of β-propeller proteins. As is the case with β-propeller proteins, the main forces that form the GFRP pentamer seem to be mediated by hydrophobic interactions at the intersubunit interfaces, which involve several nonpolar residues of the innermost, second, and third β-strands. However, the intersubunit interactions in the GFRP pentamer seem to be much tighter than those of interblade interactions of β-propeller proteins. The total buried accessible surface area for the GFRP monomer is 2,190 Å^2, which is larger than that of other β-propeller proteins (for example, 1,530 Å^2 for one repeat of tachylectin-2). Moreover, the GFRP pentamer has a much smaller central tunnel along the 5-fold axis than the classical β-propeller proteins (Fig. 4*A*). This is because of unique interactions among the central β-strands, which pack together around the central 5-fold axis. In particular, the side chains of Ser-69 and Thr-71 play key roles in intimate side-by-side interactions between each pair of β5 strands, thus forming interstrand hydrogen bonds (Fig. 4*B*). In addition, two salt bridges between Arg-11 and Glu-46 and between Arg-54 and Asp-21 stabilize the intersubunit interactions.

GFRP contains no sequence motif similar to the tryptophan-aspartic acid (34) or kelch repeats (35), both of which are popular repeats for β-propeller structures. In addition, the β-sheet topology of GFRP is different from those of the β-propeller proteins. The antiparallel β-sheets of the β-propeller proteins are formed sequentially with the N-terminal β-strand being located at the center of the propeller, that is, β1-β2-β3-β4 from the inside to the outside of the β-propeller. In contrast, the antiparallel β-sheet arrangement of GFRP is β5-β6-β1-β2 from the inside to the outside (Fig. 4*C*). Nevertheless, superposition of the inner three β-strands between GFRP and tachylectin-2 results in a relatively small value of the rms deviation for C_α atoms (0.78 Å; Fig. 4*C*). In GFRP, two helices and an antiparallel β-sheet (β3-β4) are inserted between β2 and β5 strands (Fig. 3*C*). This inserted β-sheet protrudes the connecting loop (loop β3-β4) toward the bound GTPCHI.

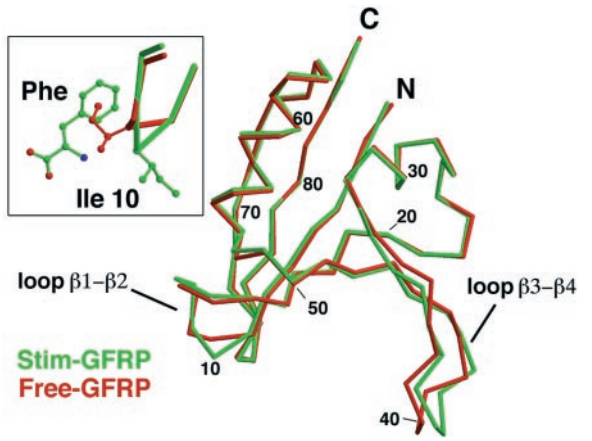

Fig. 6. Superimposition of the GFRP monomers in the stimulatory (Stim, green) and free (red) forms. (*Inset*) A close-up view around Ile-10.

GFRP-GTPCHI Interfaces. Three GFRP loops, β1-β2 (residues 9–16), β3-β4 (residues 38–45), and β5-β6 (residues 73–75), make contact with GTPCHI (Fig. 5*A*). Loop β3-β4 from the inserted β-sheet contacts one GTPCHI subunit at the outer region of the interfaces between GFRP and GTPCHI, and loops β1-β2 and β5-β6 contact the other adjacent GTPCHI subunit at the innermost region of the interfaces. Thus, one GFRP monomer makes contact with two GTPCHI subunits (Fig. 5*B*). At the innermost regions of the interfaces close to the 5-fold axis, Ile-10 and Arg-11 from loop β1-β2 and Gln-75 from loop β5-β6 make contact with the GTPCHI residues 227–230 of the N-terminal region of the C-terminal helix. These contacts are primarily due to van der Waals interactions and a salt bridge formed between Arg-11 from GFRP and Glu-227 from GTPCHI (Fig. 5*D*). At the outermost region of the interfaces, Asn-42 from GFRP loop β3-β4 forms direct and water-mediated hydrogen bonds with Glu-227 and Arg-226 from GTPCHI, respectively. In addition, two nonpolar residues, Leu-40 and Gly-41 from loop β3-β4, make hydrophobic interactions withVal-182 and Leu-222 from GTPCHI, respectively.

Phenylalanine-Binding Site. In our stimulatory complex, five L-phenylalanine molecules are located at the inner regions of the GTPCHI·GFRP interfaces (Fig. 2*C*) and are buried completely inside the interfaces. The total buried accessible surface area of each GFRP·GTPCHI interface, including these trapped five phenylalanine molecules, is increased to 6,002 Å^2, which is significantly larger than that (3,726 Å^2) without the phenylalanine molecules. Thus, phenylalanine binding enhances the association of GFRP with GTPCHI by occupying the spaces at the interfaces to increase the contact area. The GFRP pentamer forms five phenylalanine-binding cavities to accommodate the phenyl group (Fig. 5*C*), whereas the GTPCHI has no such cavity for phenylalanine (Fig. 5*A*). Recent ligand-binding studies using equilibration gel filtration (27) have indicated that phenylalanine weakly binds free GFRP but not free GTPCHI. These observations are consistent with our structure, in which the phenylalanine-binding cavity is located primarily on GFRP rather than on GTPCHI. Each binding cavity on the GFRP pentamer is located at each intersubunit region between two adjacent subunits and consists of loops β1-β2 (residues 9–13) and β5-β6 (residues 73–78) from one GFRP monomer and loop β5-β6 from the adjacent monomer. Thus, loop β5-β6 participates in the recognition of two phenylalanine molecules on both sides, although no significant cooperativity of phenylalanine binding has been observed (27). We have found a tentative potassium ion trapped inside the loop β1-β2, of which conformation seems to be stabilized by the bound potassium ion, although the ion has no direct interaction with the bound phenylalanine (Fig. 5*B*).

The phenylalanine-binding cavity is tiled with hydrophobic residues that interact with the hydrophobic phenyl group of the bound phenylalanine (Fig. 5 *D* and *E*). The amino and carboxyl groups of phenylalanine form six hydrogen bonds with GFRP. Two GFRP residues, Gln-75 and Gln-9, participate in the hydrogen-bonding interactions through their side chains; the side chain of Gln-75 from one GFRP subunit is hydrogen-bonded directly with the amino and carboxyl groups of phenylalanine, and the side chain of Gln-9 from the other GFRP subunit forms a water-mediated hydrogen bond with the amino group. This water molecule is linked also to the side chain of Glu-227 from GTPCHI, and the main-chain carbonyl group of this GTPCHI residue forms a direct hydrogen bond with the amino group of the bound phenylalanine. Thus, Glu-227 is a single key residue from GTPCHI involved in the recognition of phenylalanine.

Recently the crystal structure of the free form of GFRP, which forms a pentameric ring similar to the GFRP pentamer in our stimulatory complex, has been reported (36). The rms deviation of C_α atoms (residues 2–83) between the free and GTPCHI-bound forms of GFRP is small: 0.58 Å for monomer and 0.69 Å for pentamer. However, local but significant displacements were found in loop β1-β2 forming the phenylalanine-binding site and loop β3-β4 contacting GTPCHI (Fig. 6). Interestingly, in the

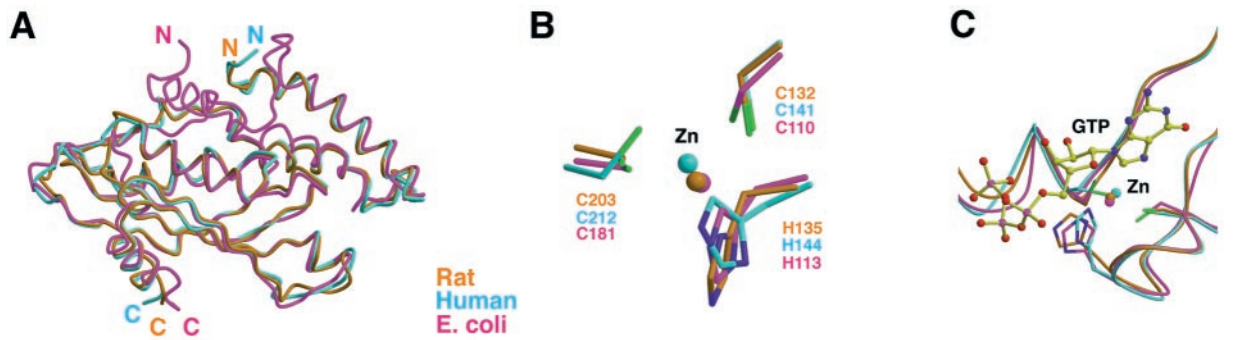

Fig. 7. The comparison of other GTPCHI structures. (*A*) Superimposed structures of the rat (orange), human (PDB code 1FB1, blue), and *E. coli* (PDB code 1FBX, magenta) GTPCHI monomers shown as tube models of C_α traces. The rat GTPCHI is from the stimulatory GTPCHI·GFRP complex, whereas the human and *E. coli* GTPCHI monomers are from the free forms. (*B*) A view of superimposed zinc ions and the ligands (two cysteines and one histidine) from GTPCHI at the active sites of the rat (orange), human (blue), and *E. coli* (magenta) GTPCHI. (*C*) A superimposed view of the active sites of rat (orange), human (blue), and *E. coli* (magenta) GTPCHI shown as tube models of C_α traces. The GTP molecule (shown as a ball-and-stick model) bound to the zinc ion-free *E. coli* GTPCHI (PDB code 1A8R) is superimposed on the structures.

free form, Ile-10 at loop β1-β2 is flipped toward the hydrophobic cavity, which is occupied with the phenylalanine aromatic ring in the stimulatory complex. No significant structural change is found in a short GTPCHI-contacting loop β5-β6. The potassium ions are observed also at the same position in the free GFRP structure.

GTPCHI Structure. The rat GTPCHI monomer is comprised of six α-helices and a four-stranded antiparallel β-sheet. Superposition of the rat and human GTPCHI monomers results in a relatively small rms deviation of 0.90 Å (Fig. 7*A*). The four-stranded β-sheet of the monomer forms a 20-stranded antiparallel β-barrel in each pentamer by tight association between the N- and C-terminal strands of each adjacent subunit. The two pentamers are associated in a head-to-head manner to form the active decameric enzyme complex with pseudo 52-point group symmetry. These structural characteristics are essentially the same as those found in the free forms of truncated human and *E. coli* GTPCHI decamers (18, 26). As observed in these *E. coli* and human enzymes, each rat GTPCHI monomer contains one zinc ion, which binds conserved Cys-132, His-135, and Cys-203 at the active site (Fig. 7*B*). Superposition of the decamers of these enzymes also gives a small rms deviation of 1.07 Å; no significant structural changes were found at the active site (Fig. 7 *B* and *C*). Because the *E. coli* enzyme shows no cooperativity, and thus only one active form exists, the structural similarity observed between the *E. coli* GTPCHI and our GTPCHI in the stimulatory complex suggests that GFRP locks the enzyme in the active form. A better understanding of the allosteric regulation of GTPCHI by GFRP will be provided by a future structural comparison between the stimulatory and inhibitory complexes.

We thank J. Tsukamoto for technical support in performing the matrix-assisted laser desorption ionization/time-of-flight MS analysis, Drs. N. Igarashi, M. Suzuki at Photon Factory (BL 6a and 18b), and M. Kawamoto at SPring-8 (BL41XU) for data collection. We also thank Dr. T. Shimizu for advice on the data reduction and help with the analyses. This work was supported by National Institutes of Health Grant DK51257 (to K.H.) and Grants-in-aid for the Encouragement of Young Scientists 13780535 (to K.O.), for Scientific Research B (12490024), and in Priority Areas B on Metal Sensor 12147206 (to T.H.) from the Ministry of Education, Culture, Sports, Science and Technology of Japan. T.H. is a member of the Structural Biology Sakabe project of the Foundation for Advancement of International Science.

1. Niederwieser, A., Blau, N., Wang, M., Joller, P., Atares, M. & Cardesa, J.-G. (1984) *Eur. J. Pediatr.* **141,** 208–214.
2. Ichinose, H., Ohye, T., Matsuda, Y., Hori, T., Blau, N., Burlina, A., Rouse, B., Matalon, R., Fujita, K. & Nagatsu, T. (1995) *J. Biol. Chem.* **270,** 10062–10071.
3. Nygaard, T. G. (1995) *Curr. Opin. Neurobiol.* **8,** 310–313.
4. Ichinose, H., Ohye, T., Takahashi, E., Seki, N., Hori, T., Segawa, M., Nomura, Y., Endo, K., Tanaka, H., Tsuji, S., Fujita, K. & Nagatsu, T. (1994) *Nat. Genet.* **8,** 236–242.
5. Cosentino, F., Patton, S., d'Uscio, L. V., Werner, E. R., Werner, G.-F., Moreau, P., Malinski, T. & Luscher, T. F. (1998) *J. Clin. Invest.* **101,** 1530–1537.
6. Stroes, E., Kastelein, J., Cosentino, F., Erkelens, W., Wever, R., Koomans, H., Luscher, T. & Rabelink, T. (1997) *J. Clin. Invest.* **99,** 414–416.
7. Piper, G. M. (1997) *J. Cardiovasc. Pharmacol.* **29,** 8–15.
8. Meininger, C. J., Marinos, R. S., Hatakeyama, K., Martinez, R.-Z., Rojas, J. D., Kelly, K. A. & Wu, G. (2000) *Biochem. J.* **348,** 353–356.
9. Lovenberg, W., Levine, R. A., Robinson, D. S., Ebert, M., Williams, A. C. & Calne, D. B. (1979) *Science* **204,** 624–626.
10. LeWitt, P. A., Levine, R. A., Lovenberg, W., Pomara, N., Stanley, M., Gurevich, D., Schlick, P. & Roberts, R. (1986) in *Strategies for Research and Development*, eds. Fisher, A., Hanin, I. & Lachman, C. (Plenum, New York) pp. 323–327.
11. Yoneyama, T., Wilson, L. & Hatakeyama, K. (2001) *Arch. Biochem. Biophys.* **388,** 67–73.
12. Harada, T., Kagamiyama, H. & Hatakeyama, K. (1993) *Science* **260,** 1507–1510.
13. Yoneyama, T. & Hatakeyama, K. (1998) *J. Biol. Chem.* **273,** 20102–20108.
14. Hatakeyama, K., Harada, T., Suzuki, S., Watanabe, Y. & Kagamiyama, H. (1989) *J. Biol. Chem.* **264,** 21660–21664.
15. Hatakeyama, K., Inoue, Y., Harada, T. & Kagamiyama, H. (1991) *J. Biol. Chem.* **266,** 765–769.
16. Yoneyama, T., Brewer, J. M. & Hatakeyama, K. (1997) *J. Biol. Chem.* **272,** 9690–9696.
17. Maita, N., Okada, K., Hirotsu, S., Hatakeyama, K. & Hakoshima, T. (2001) *Acta Crystallogr. D* **57,** 1153–1156.
18. Nar, H., Huber, R., Meining, W., Schmid, C., Weinkauf, S. & Bacher, A. (1995) *Structure (London)* **3,** 459–466.
19. Navaza, J. & Vernoslava, E. (1995) *Acta Crystallogr. A* **51,** 445–449.
20. Collaborative Computational Project, Number 4 (1994) *Acta Crystallogr. D* **50,** 760–763.
21. Jones, T. A., Zou, J. Y., Cowan, S. W. & Kjeldgaard, M. (1991) *Acta Crystallogr. A* **47,** 110–119.
22. Brünger, A. T., Adams, P. D., Clore, G. M., DeLano, W. L., Gros, P., Grosse, R. W.-K., Jiang, J. S., Kuszewski, J., Nilges, M., Pannu, N. S., *et al*. (1998) *Acta Crystallogr. D* **54,** 905–921.
23. Kraulis, P. J. (1991) *J. Appl. Crystallogr.* **24,** 946–950.
24. Merritt, E. A. & Bacon, D. J. (1997) *Methods Enzymol.* **277B,** 505–524.
25. Nicholls, A., Sharp, K. & Honig, B. (1991) *Proteins* **11,** 281–296.
26. Auerbach, G., Herrmann, A., Bracher, A., Bader, G., Gütlich, M., Fischer, M., Neukamm, M., Garrido, M.-F., Richardson, J., Nar, H., Huber, R. & Bacher, A. (2000) *Proc. Natl. Acad. Sci. USA* **97,** 13567–13572. (First Published November 21, 2000; 10.1073/pnas.240463497)
27. Yoneyama, T. & Hatakeyama, K. (2001) *Protein Sci.* **10,** 871–878.
28. Murzin, A. G., Brenner, S. E., Hubbard, T. & Chothia, C. (1995) *J. Mol. Biol.* **247,** 536–540.
29. Holm, L. & Sander, C. (1993) *J. Mol. Biol.* **233,** 123–138.
30. Cort, J. R., Koonin, E. V., Bash, P. A. & Kennedy, M. A. (1999) *Nucleic Acids Res.* **27,** 4018–4027.
31. Beisel, H. G., Kawabata, S., Iwanaga, S., Huber, R. & Bode, W. (1999) *EMBO J.* **18,** 2313–2322.
32. Sondek, J., Bohm, A., Lambright, D. G., Hamm, H. E. & Sigler, P. B. (1996) *Nature (London)* **379,** 369–374.
33. Fülöp, V. & Jones, D. T. (1999) *Curr. Opin. Struct. Biol.* **6,** 715–721.
34. Smith, T. F., Gaitatzes, C., Saxena, K. & Neer, E. J. (1999) *Trends Biochem. Sci.* **24,** 181–185.
35. Adams, J., Kelso, R. & Cooley, L. (2000) *Trends Cell Biol.* **10,** 17–24.
36. Bader, G., Schiffmann, S., Herrmann, A., Fischer, M., Gütlich, M., Auerbach, G., Ploom, T., Bacher, A., Huber, R. & Lemm, T. (2001) *J. Mol. Biol.* **312,** 1051–1057.